Applied Catalysis B: Environmental 256 (2019) 117826

Contents lists available at ScienceDirect

Applied Catalysis B: Environmental

journal homepage: www.elsevier.com/locate/apcatb

Catalytic conversion of cellulose to sorbitol over Ru supported on biomass-derived carbon-based materials

Natalia Rey-Raap*,[1], Lucília Sousa Ribeiro*,[1], José J. de Melo Órfão, José L. Figueiredo, Manuel Fernando Ribeiro Pereira

Associate Laboratory LSRE-LCM, Departamento de Engenharia Química, Faculdade de Engenharia, Universidade do Porto, R. Dr. Roberto Frias s/n, 4200-465 Porto, Portugal

ARTICLE INFO

Keywords:
Glucose-based materials
Ru-catalysts
Cellulose
Hydrolytic hydrogenation
Sorbitol

ABSTRACT

The direct conversion of cellulose into sorbitol, one of the platform molecules of highest potential, by using a low-cost catalyst that yields higher productivity is a current challenge. Ruthenium/glucose-derived carbons with tailored textural and chemical properties were prepared by combining two different strategies: activation and addition of carbon nanotubes (CNT) to obtain a hybrid carbon material (AG-CNT). The appropriate combination of both strategies results in materials with high microporosity and low acidity that favors the dispersion of the metal and, hence, improves the yield of sorbitol. The total conversion of cellulose (100%) and the highest yield of sorbitol (64.1%) were achieved over a hybrid catalyst with high specific surface area of 1200 $m^2 g^{-1}$ (Ru/AG-CNT_{1200}) within 3 h of reaction, at 205 °C and 50 bar of H_2. In addition, the catalyst was successfully recycled in four runs. These results are better than those reported over Ru/CNT (the highest yield reported to date over carbon supports) under the same reaction conditions, indicating that CNT can be successfully replaced by a low-cost support derived from biomass. As a result, not only the highest yield of sorbitol is obtained, but cellulose, one of the most important fractions of biomass, is valorized through two pathways: the cellulose itself as the main raw material of the reaction and its monomer, glucose, for the preparation of the catalyst.

1. Introduction

The use of biomass for the production of chemical compounds is an essential strategy to achieve a more sustainable and green economy. The formation of platform molecules from biomass through low-temperature processes is widely used to obtain high added value chemical products [1–3]. Sorbitol is one of the most promising platform molecules included in the list of the twelve building block chemicals of highest potential derived from biomass [4]. Indeed, sorbitol is nowadays industrially produced from the hydrogenation reaction of glucose using Raney Nickel catalysts, and its production is expected to reach 2.34 million tons by 2020 [5,6]. However, the existence of a commercial catalytic process must not preclude the pursuit of performing further research that could result in a relevant contribution to fundamental scientific knowledge and in interesting improvements of the process: higher productivity and lower costs.

One of the main challenges in the production of sorbitol is the high cost involved in processing the raw materials, particularly from the conversion of cellulose to glucose and subsequent separation from subproducts. Therefore, many efforts have been made to achieve the direct conversion of cellulose into sorbitol [7,8]. The main advantage of this process compared to the conventional method is that the separation process of intermediate products is avoided, resulting in a more competitive process. This direct conversion of cellulose into sorbitol involves two main reactions: i) hydrolysis of cellulose to glucose favored by the presence of acidic sites and ii) subsequent hydrogenation of glucose to sorbitol over metal catalysts [6]. In addition to the role of the acidic sites, it should be noted that cellulose is a robust compound, and harsh conditions are required to break its bonds and to produce glucose molecules. Several studies have demonstrated that reducing the crystallinity of cellulose leads to a more reactive structure. The pretreatments of cellulose with ionic liquids, acid solutions or by milling processes, have been shown to be excellent strategies to decrease the crystallinity of cellulose [4,9–12], and hence, to increase its conversion to glucose. As aforementioned, the subsequent hydrogenation of glucose to sorbitol has been commonly performed on nickel based catalysts due to their low cost and high activity [5,13–15]. However, leaching problems associated to nickel catalysts have led to the study of other

* Corresponding authors.
E-mail addresses: nataliarey@fe.up.pt (N. Rey-Raap), lucilia@fe.up.pt (L.S. Ribeiro).
[1] Both authors contributed equally to this work.

https://doi.org/10.1016/j.apcatb.2019.117826
Received 25 January 2019; Received in revised form 29 May 2019; Accepted 5 June 2019
Available online 06 June 2019
0926-3373/ © 2019 Elsevier B.V. All rights reserved.

Table 1
Yields of sorbitol as a function of the reaction conditions.

Commercial Carbon Support	Ruthenium loading (wt.%)	Catalyst/reagent ratio	Reaction conditions	Yield of sorbitol	Reference
Activated carbon	3 wt.%	1:2.3	16 bar, 180 °C, 3 h 1100 rpm	89 %	[25]
Activated carbon	10 wt.%	1:2.5	50 bar, 165 °C, 36 h 450 rpm	71 %	[11]
Activated carbon	0.4 wt.%	1:2.5	50 bar, 205 °C, 5 h 150 rpm	42 %	[24]
Carbon nanotubes	1 wt.%	1:3.2	50 bar, 185 °C, 24 h –	69 %	[12]
Carbon nanotubes	0.4 wt.%	1:2.5	50 bar, 205 °C, 5h 150 rpm	51 %	[26]

metals such as Ru, Rh, Pt or Pd [16–20]. Most of the metal-based catalysts used are supported on inorganic carriers, such as zeolites, titania, alumina, zirconia, and alloys or mixtures of different oxides [13,16,17,19–23], reaching yields of sorbitol higher than 90%. However, many of these catalysts deactivate after less than 10 cycles of reuse. In this context, carbon materials are particularly promising catalyst supports due to their high chemical stability. Carbon materials such as graphene, carbon nanotubes (CNT), carbon nanofibers and activated carbons have been used as metal supports for the conversion of cellulose to sorbitol [9,11,12,15,24–27]. Among them, ruthenium catalysts supported on activated carbons and carbon nanotubes were shown to be the most effective supports for the direct conversion of cellulose to sorbitol, reaching yields of sorbitol up to 89% and 69%, respectively. However, it should be highlighted that such high yields of sorbitol were obtained after long reaction times or by using high metal loadings or expensive carbon supports (Table 1), which could limit their industrial application. Therefore, it is necessary to develop new catalysts supported on low-cost carbons that result in a high production of sorbitol in a short reaction time. In this context, the use of biomass as the carbon source for the supports appears as an interesting alternative.

Hydrothermal carbonization (HTC) of biomass has received much attention in recent years as a methodology to obtain biomass-derived carbons, due to its low cost and mild synthesis conditions that makes the process affordable and environmentally friendly [28]. However, one of the main drawbacks of hydrothermal carbons is that they usually exhibit limited or inadequate textural and chemical properties that may affect the catalytic performance. Strategies to obtain the most adequate properties that give rise to enhanced catalytic performance should therefore be defined, as catalytic results depends to a great extent on the textural and chemical properties of the support and the nature of the catalyst. Some studies suggest that there is not an obvious correlation between the catalytic performance of sorbitol formation and the specific surface area when carbon nanotubes or graphene are used as supports [12,26,27], while other studies state that, for porous supports, higher surface areas result in higher catalytic activities [8,13,22,29]. The latter could be due to porosity affecting the dispersion and size of metal particles [23,29], and hence, the decisive factor in the catalytic reaction would be the intrinsic activity of the metal rather than the specific surface area of the support; or microporosity may contribute as active sites itself. On the other hand, the acidity of the support is also expected to favor the conversion of cellulose to glucose [11,26,30–32], while it does not seem to favor the conversion of glucose to sorbitol [25,26]. Accordingly, a balance in the acidity of the supports should be found in order to obtain the highest conversion of cellulose and the highest yield of sorbitol.

Many of the differences mentioned above are related to the use of supports of diverse nature that hinder comparisons and make it difficult to design new supports. Therefore, the design of biomass-derived carbons supports for the one-pot conversion of cellulose to sorbitol is a current challenge, and hence, an in-depth study focused on the effect of the textural and chemical properties of the biomass-derived carbon supports is needed. Accordingly, in the present study ruthenium catalysts supported on carbon materials with different chemical and textural properties were prepared. Carbon supports were obtained by the hydrothermal carbonization of glucose, one of the main fractions of biomass. The properties of the materials were modified by following two strategies: i) adding carbon nanotubes during the hydrothermal carbonization and ii) applying different thermal treatments to the hydrothermal carbons: carbonization and physical activation. Through this approach, high yields of sorbitol were obtained while valorizing at the same time glucose for the preparation of the catalyst support and cellulose as the main raw material of the reaction.

2. Materials and methods

2.1. Chemicals and materials

The selected starting precursors used in the preparation of the supports were D-glucose (99.5%, from Alfa Aesar, Karlsruhe, Germany), multiwalled carbon nanotubes (NANOCYL™ NC3100 series, with average diameter of 9.5 nm, average length of 1.5 μm and carbon purity higher than 95%, supplied by Nanocyl, Sambreville, Belgium) and deionized water (from a Panice reverse osmosis water system). The metal precursor ruthenium (III) chloride ($RuCl_3$ 99.9%, Ru 38% min.) used in the preparation of the catalysts and the microcrystalline cellulose, main raw material of the reaction, were purchased from Alfa Aesar, Karlsruhe, Germany. Ultrapure water with a conductivity of 18.2 μS cm^{-1} obtained in a Milli-Q Millipore system was used for the preparation of all solutions in the catalytic experiments. Unlike cellulose, which was ball-milled at a frequency of 20 s^{-1} for 4 h using a Retsch Mixer Mill MM200 equipment to reduce its crystallinity [10], all chemicals were used as received without further purification.

2.2. Preparation of supports

Two different supports were prepared by hydrothermal carbonization (HTC): i) a glucose-based material and ii) a glucose/carbon nanotube hybrid. Glucose (in the case of non-hybrid samples) and carbon nanotubes (in the case of hybrid samples) were first dispersed in deionized water under sonication for around 30 min at room temperature. The solid/water ratio (*w/v*) was fixed at 1:5 for all experiments, while the amount of CNT added was fixed at 2 wt.%. After sonication, each solution/suspension was transferred to a sealed Teflon-lined autoclave and heated to 180 °C for 12 h. The autoclave was cooled down to room temperature and then the solid product was recovered by filtration, washed with abundant deionized water and dried at 80 °C for 24 h. Dried samples were carbonized in N_2 (99.999% from Linde, Portugal) and activated using CO_2 (99.8% from Linde, Portugal) as the activating agent in a vertical furnace under the conditions shown in Table 2. The heating rate was fixed at 10 °C min^{-1} for all experiments. Supports were named CG or AG denoting samples prepared by carbonization or activation, respectively. The name of the activated samples

Table 2
Experimental conditions employed for the preparation of the samples.

Sample	Type of gas / gas flow	Temperature (ºC)	Time (h)
CG	N_2 / 50 $cm^3 min^{-1}$	700	2
AG_{600}	CO_2 / 80 $cm^3 g^{-1} min^{-1}$	700	2
AG_{1000}	CO_2 / 80 $cm^3 g^{-1} min^{-1}$	900	2
AG_{2200}	CO_2 / 80 $cm^3 g^{-1} min^{-1}$	900	6
CG-CNT	N_2 / 50 $cm^3 min^{-1}$	700	2
$AG\text{-}CNT_{700}$	CO_2 / 80 $cm^3 g^{-1} min^{-1}$	700	2
$AG\text{-}CNT_{1200}$	CO_2 / 80 $cm^3 g^{-1} min^{-1}$	900	2
$AG\text{-}CNT_{1400}$	CO_2 / 80 $cm^3 g^{-1} min^{-1}$	900	6

is followed by the value of the surface area measured (values in $m^2 g^{-1}$) as detailed below. Hybrid samples are also labelled with the abbreviation CNT in reference to the presence of carbon nanotubes.

2.3. Preparation of catalysts

All catalysts were prepared by the incipient wetness impregnation method of the previously prepared glucose-based materials (Section 2.2) with a solution of the Ru precursor. The amount of ruthenium was calculated to achieve a nominal metal loading of 0.4 wt. % [18]. After the impregnation, the resulting materials were dried overnight in an oven at 110 °C. Then, the catalysts were heat treated under a nitrogen flow of 50 $cm^3 min^{-1}$ at 250 °C for 3 h and subsequently reduced under a hydrogen flow of 50 $cm^3 min^{-1}$ at 250 °C for 3 h. The prepared catalysts were denoted as Ru/X, where X is the name of the corresponding support shown in Table 2.

2.4. Characterization of supports and catalysts

The textural and chemical properties of the supports were determined by nitrogen adsorption-desorption isotherms, elemental analysis and temperature programmed desorption (TPD). The N_2 adsorption-desorption isotherms were performed at -196 °C using a Quantachrome Autosorb iQ automated gas sorption analyser. Prior to analysis, all samples were degassed under vacuum at 150 °C overnight. The specific surface area (S_{BET}) was calculated by applying the Brunauer-Emmett-Teller (BET) equation to the nitrogen adsorption branch of the isotherm. The micropore volume (V_{DR}) was evaluated by means of the Dubinin-Raduskevich method and the total pore volume (V_P) was determined from the volume of nitrogen adsorbed at saturation point. The external surface area (non-microporous surface [33]) was calculated following the procedure detailed in reference [34]. The pore size distribution was also evaluated from isotherm data by applying the Quench Solid Density Functional Theory (QSDFT), which takes into account the effects of surface roughness and heterogeneity.

The elemental analysis was carried out in a Vario Micro Cube analyser from Elementar. This technique involves the combustion of the sample at a temperature close to 1000 °C in an oxygen-rich atmosphere. Analysis of the combustion products allows to determine the contents of C, H, N and S. The oxygen content is determined by difference. In addition, the nature and amount of surface oxygenated groups were evaluated by TPD. The analyses were carried out in an Altamira Instruments AMI-300 equipment with a mass spectrometry detector (Dycor Dymaxion). The samples (70 mg) were loaded into a U-shaped quartz cell and heated from room temperature to 1000 °C under a flow of helium. The heating and flow rates were fixed at 5 °C min^{-1} and 25 $cm^3 min^{-1}$, respectively. The calibration of CO_2 and CO was performed at the end of each analysis in order to quantify the amounts of these gases released during the TPD experiments.

The textural properties of the supported catalysts were also characterized by nitrogen adsorption-desorption isotherms, following the same experimental conditions used for the characterization of the supports. In addition, the morphology of the samples was examined with a Quanta FEG 400 scanning electron microscope (FEI Company) and a transmission electron microscope JEOL JEM2010. In the former, the samples were previously attached to an aluminum pin using conductive double-sided adhesive tape. An accelerating voltage of 15 kV and a secondary electron detector Everhart-Thornley (ETD) were used in all the analyses. For the transmission electron microscopy, samples were first dissolved in ethanol and then deposited over a carbon grid. Particle size distribution was determined by measuring at least 100 particles, and the average diameter was determined by $d_p = \sum d_i n_i / \sum n_i$ (where n_i is the number of particles with diameter d_i). The chemical surface functionalities of the ruthenium supported catalysts were analyzed by X-ray photoelectron spectroscopy (XPS). The XPS analyses were performed using a Kratos AXIS Ultra HSA, with VISION software for data acquisition and CASAXPS software for data analysis. The analysis was carried out with a monochromatic Al Kα X-ray source (1486.7 eV), operating at 15 kV in hybrid mode, with a pass energy of 40 eV for regions of interest and 80 eV for survey. The loading of Ru was determined by means of an inductive coupled plasma emission spectrometer (Perkin Elmer Optima 4300 DV).

2.5. Catalyst evaluation

A 1000 mL stainless steel Parr reactor (Parr Instruments, USA Mod. 5120) was used for all catalytic tests at 50 bar of H_2 (99.999% from Linde, Portugal) for 5 h. Typically, 750 mg of ball-milled cellulose, 300 mg of catalyst and 300 mL of water were introduced inside the reactor under stirring at 150 rpm. Preliminary studies had confirmed no mass transfer limitations (neither internal or external) under the conditions selected in the present study. Then, the reactor was sealed, purged three times with N_2 to remove air and heated to the desired temperature (205 °C). After heating, the reaction was initiated by switching from N_2 to H_2 (50 bar). Samples were collected at selected times, filtrated, centrifuged at 13,500 rpm for 10 min and decanted prior to analysis. At the end of the reaction, the catalyst was recovered by filtration.

The liquid products were analysed by high performance liquid chromatography (HPLC) using two different detectors: an ultraviolet detector at 210 nm and a refractive index (RI) detector. The different products were separated using an ion exclusion column (Alltech OA-1000) with a 5 mmol L^{-1} H_2SO_4 (> 95%, from VWR, Alfragide, Portugal) mobile phase at 0.5 mL min^{-1}. The yield (Y_i) of each product i was calculated according to the following equation:

$$Y_i\ (\%) = \frac{moles\ of\ product\ i\ formed\ (measured\ by\ HPLC) \times C\ atoms\ in\ product\ i}{moles\ of\ C\ in\ cellulose\ initially\ present} \times 100 \quad (1)$$

The conversion (X) of cellulose was determined on the basis of total organic carbon (TOC) data (Shimadzu TOC 5000-A), using the following equation:

$$X\ (\%) = \frac{total\ moles\ of\ organic\ carbon\ in\ resultant\ liquid}{moles\ of\ carbon\ in\ cellulose\ charged\ into\ reactor} \times 100 \quad (2)$$

Conversions and yields in the catalytic experiments had typical absolute errors of ± 3% and ± 1%, respectively.

2.6. Stability test

The stability of a catalyst is a very important condition to consider in continuous production processes, particularly from an environmental and industrial point of view. Therefore, the recyclability of the most efficient catalyst was examined. After the first reaction, the solid (corresponding to the catalyst, since cellulose conversion was 100%) was separated from the reaction solution (water and soluble products) by centrifugation and filtration. Then, the recovered catalyst was washed and dried, and tested again under the same reaction conditions by adding fresh cellulose feed. Due to some losses during the recovering

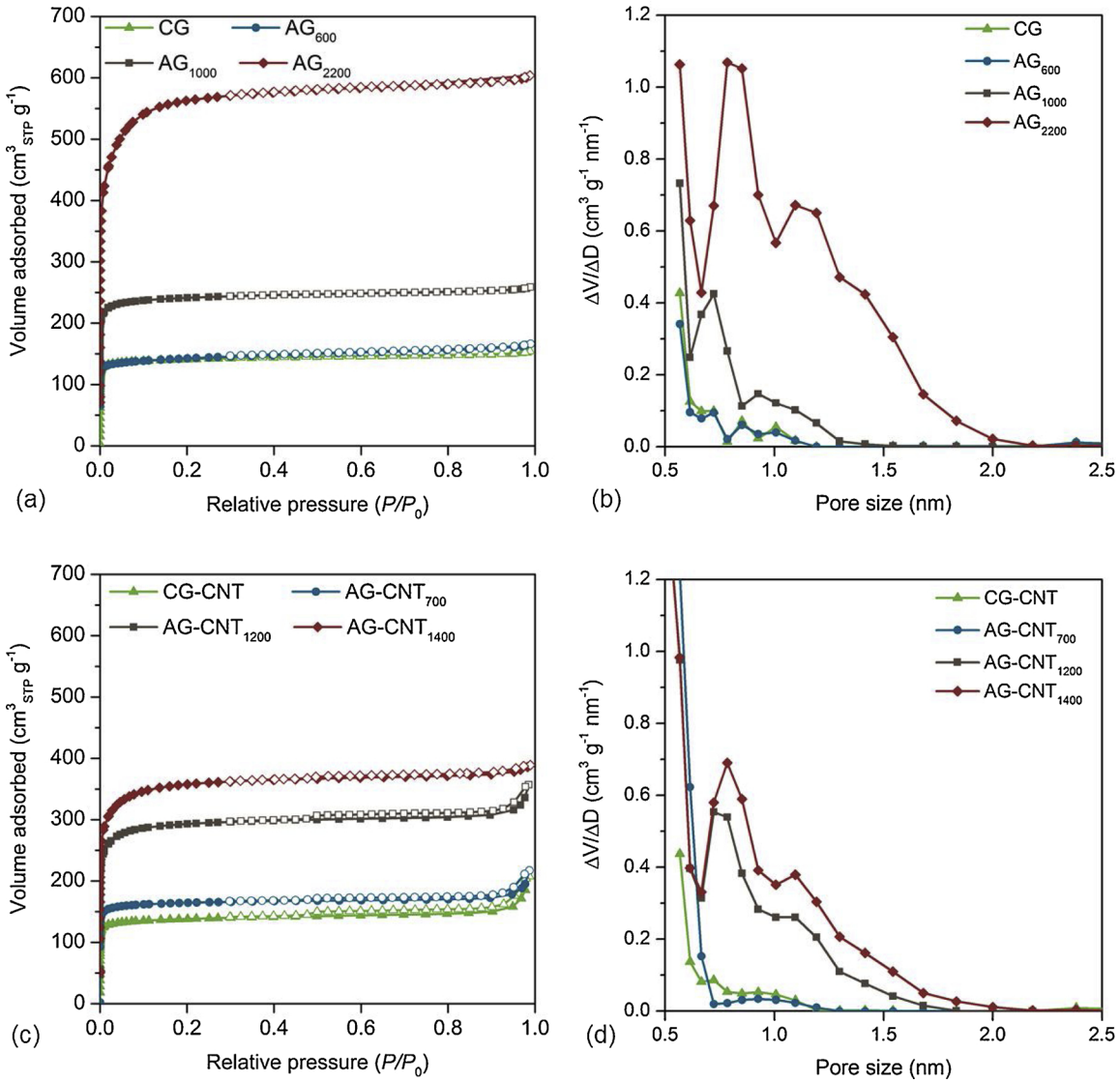

Fig. 1. N_2 adsorption/desorption isotherms at -196 °C and pore size distributions for glucose-derived (a) and (b), and hybrid carbons (c) and (d), respectively.

process, a small amount of fresh catalyst (< 5 wt. %) was also added before each test.

3. Results and discussion

3.1. Characterization of supports

N_2 adsorption-desorption isotherms of glucose-derived carbon supports are shown in Fig. 1a and c. All the prepared materials display a type I isotherm according to the IUPAC classification, which is characteristic of microporous solids. The most important textural parameters calculated from the analysis of the isotherms are compiled in Table 3.

The isotherm of sample CG, shown in Fig. 1a, is concave to the relative pressure axis and increases rapidly at low relative pressures, which indicates the presence of micropores (Table 3). Activation under the same conditions than those used during carbonization (700 °C, 2 h) results in a material with a similar porous structure (sample AG_{600} and CG, respectively), suggesting that, at such conditions, the influence of the CO_2 atmosphere used during activation is negligible. However, a further inspection of the isotherms presented in Fig. 1a reveals a noticeable increase in microporosity due to an increase in the temperature and time of activation applied (Table 3). During activation, CO_2 reacts with the carbon structure resulting in the extraction of carbon atoms. This reaction occurs after many collisions between CO_2 molecules and the internal surface of the carbon [35]. Therefore, an increase in the time of activation results in a higher number of collisions that give rise to the extraction of more carbon atoms. The development of porosity during this process may be explained by three main mechanisms, related to the site where the extracted carbon atom was previously placed: i) opening of previously inaccessible pores, ii) widening of existing pores, and iii) creation of new pores [35]. These effects are corroborated by the pore size distribution shown in Fig. 1b and d, in which it can be observed that the volume and size of the pores increase with the degree of activation. In addition, the opening and widening of pores also produce an increase in the external surface area of the supports (non-microporous surface [33]).

The volume of N_2 adsorbed at low relative pressures barely decreases by adding CNT (sample CG-CNT in Fig. 1c), which results in a hybrid carbon material with a microporosity similar to that of sample CG. Alike in samples without CNT, activation under the same conditions as those used during carbonization results in a material with similar surface area (671 $m^2 g^{-1}$ for sample $AG\text{-}CNT_{700}$) and the microporosity increases by increasing temperature and time of activation (Table 3). Besides, hybrid samples exhibit a small hysteresis loop which appears as a result of the capillary condensation at medium-high

Table 3
Textural properties and elemental analysis of the carbon supports.

Sample	N_2 adsorption-desorption isotherm				Elemental analysis		
	S_{BET} ($m^2 g^{-1}$)	V_{DR} ($cm^3 g^{-1}$)	V_p ($cm^3 g^{-1}$)	S_{ext} ($m^2 g^{-1}$)	C (%)	H (%)	O (%)
CG	573	0.22	0.24	13	94.9	1.0	4.1
AG_{600}	571	0.23	0.26	18	95.3	0.8	3.9
AG_{1000}	984	0.37	0.40	19	96.3	0.4	3.3
AG_{2200}	2214	0.91	0.93	30	97.3	0.3	2.4
CG-CNT	559	0.22	0.32	18	95.1	1.1	3.8
AG-CNT_{700}	671	0.26	0.33	20	95.4	0.8	3.8
AG-CNT_{1200}	1175	0.47	0.55	32	96.9	0.5	2.6
AG-CNT_{1400}	1413	0.57	0.60	34	98.1	0.3	1.6

pressures, commonly observed for materials that bear mesopores in their interparticle spaces, like carbon nanotubes. However, differences in the generation of microporosity during activation can be observed due to the presence of CNT. Hybrid samples activated during 2 h at 700 °C and 900 °C exhibit higher microporosity than those without CNT: AG-CNT_{700} and AG-CNT_{1200} vs. AG_{600} and AG_{1000}, respectively. However, a further increase in the time of activation up to 6 h gave rise to a hybrid material with lower microporosity than its counterpart without CNT (AG-CNT_{1400} vs. AG_{2200}). This effect can be explained by the fact that CO_2 is more likely to react with glucose particles than with CNT due to the higher reactivity of glucose, and hence, the proportion between glucose-derived carbon particles and CNT decreases, resulting in a material with an overall lower microporosity. Like in samples without CNT, the external surface area of the hybrid materials increases with the degree of activation.

Likewise, both the activation under CO_2 atmosphere and the presence of CNT during the polymerization of glucose had an effect on the chemical properties of the carbon supports. The elemental analysis data indicate that supports consist mainly of carbon and oxygen, as shown in Table 3. The percentage of oxygen calculated by difference is around 1.6–4.1 %, which is within the range typically observed in carbon materials after carbonization or physical activation. Regardless of the presence of CNT, an increase in temperature and time of activation results in lower oxygen content attributed to the higher degree of activation. Interestingly, the presence of CNT during the polymerization of glucose also gives rise to less oxygen-rich materials. This phenomenon could be due to i) interactions between CNT and the oxygen functional groups on glucose structure during the polymerization or ii) the presence of non-functionalized CNT on the overall mass of the sample that results in a decrease of the percentage of total oxygen.

In order to get more fully acquainted with the chemical composition of the samples, the nature of the oxygen-containing functionalities was analyzed by temperature programmed desorption experiments (TPD). The total amounts of CO and CO_2 released and the percentage of oxygen were calculated from the corresponding TPD profiles and the values obtained are compiled in Table 4, along with the values of the CO/CO_2 ratio. In addition, to delve deeper into the nature of the oxygen-containing functional groups released, the deconvolution of the TPD profiles into individual components was performed [36,37]. The CO_2 (carboxylic acids, anhydrides, lactones) and CO (anhydrides, phenols, carbonyls) desorption profiles are shown in Fig. 2, whereas the results of the deconvolution of each sample are shown in Figures S1-S2 and Tables S1-S2 in the supporting information. The phenol/quinone ratio obtained from the deconvolution of the CO profile is also shown in Table 4.

Irrespective of the presence of CNT, the amounts of CO and CO_2 released, as well as the oxygen content, decrease by increasing the degree of activation of the samples, which is in agreement with the results obtained from elemental analysis (Table 3). Likewise, the amount of oxygen-containing functional groups is lower in samples bearing carbon nanotubes. The amount of CO released is much larger than that of CO_2 for all samples, although two interesting differences on

Table 4
Total amounts of CO and CO_2 released and percentage of oxygen content, obtained by integration of the areas under the TPD profiles, and the CO/CO_2 and phenol/carbonyl-quinone ratios for the carbon supports.

Sample	CO (μmol g^{-1})	CO_2 (μmol g^{-1})	Oxygen (% wt.)	CO/CO_2	Phenol/carbonyl-quinone
CG	1462	365	3.5	4.0	0.61
AG_{600}	1334	268	3.0	5.1	0.57
AG_{1000}	1111	172	2.3	6.5	0.56
AG_{2200}	971	136	2.0	7.2	0.50
CG-CNT	1185	345	3.0	3.4	0.40
AG-CNT_{700}	1139	247	2.6	4.6	0.41
AG-CNT_{1200}	831	157	1.8	5.3	0.49
AG-CNT_{1400}	548	169	1.4	3.2	0.81

the values of the CO/CO_2 ratio are observed: i) the CO/CO_2 ratio for glucose-derived carbons is higher than that of the hybrid materials and, ii) the CO/CO_2 ratio for glucose-derived carbons increases with the degree of activation, while in hybrid carbons, the sample with the higher degree of activation exhibits a CO/CO_2 ratio lower than those obtained for the rest of the hybrid materials, especially for sample AG-CNT_{1400}. This result suggests differences in the acidity of the oxygen functional groups on the surface of the supports, which is in agreement with the results of the deconvolution of the TPD profiles and the values of phenol/carbonyl-quinone ratio.

The deconvolution of the CO_2 profile of sample CG results in three broad peaks at temperature ranges of 100–400 °C, 300–650 °C and 550–800 °C, attributed to carboxylic acids, carboxylic anhydrides and lactone groups, respectively (Figure S1a) [38,39]. The contribution of the carboxylic acids and carboxylic anhydrides decreases and shifts to higher temperatures as the degree of activation increases, suggesting a more stable chemical structure. In addition, a noticeable amount of lactones is observed for sample AG_{600}, while this functional group disappears for samples with a higher degree of activation. This result suggests that the CO_2 atmosphere used during activation at low temperature (700 °C) can promote the formation of lactones, which are then released by activating at higher temperature (900 °C). As expected, the same contribution of the carboxylic anhydride groups is observed in the CO profile for all samples. Moreover, two prominent peaks at temperatures ranging from 500 to 800 °C and from 600 to 1000 °C, assigned to phenols and carbonyl-quinone groups [37,40], respectively, are also detected. As in the CO_2 profile, all the peaks in the CO profile appear at higher temperatures by increasing the temperature and time of activation, which suggests higher basicity of the surface [39]. The lower acidity of the samples by increasing the degree of activation is also supported by the decrease in the phenol/carbonyl-quinone ratio from 0.61 to 0.50 (Table 4).

The TPD profile of the hybrid sample CG-CNT is similar to that of sample CG, although certain differences are also observed. The peaks in the CO_2 and CO profiles for sample CG-CNT appear at higher temperatures (Fig. 2c and d), which can be attributed to a more stable

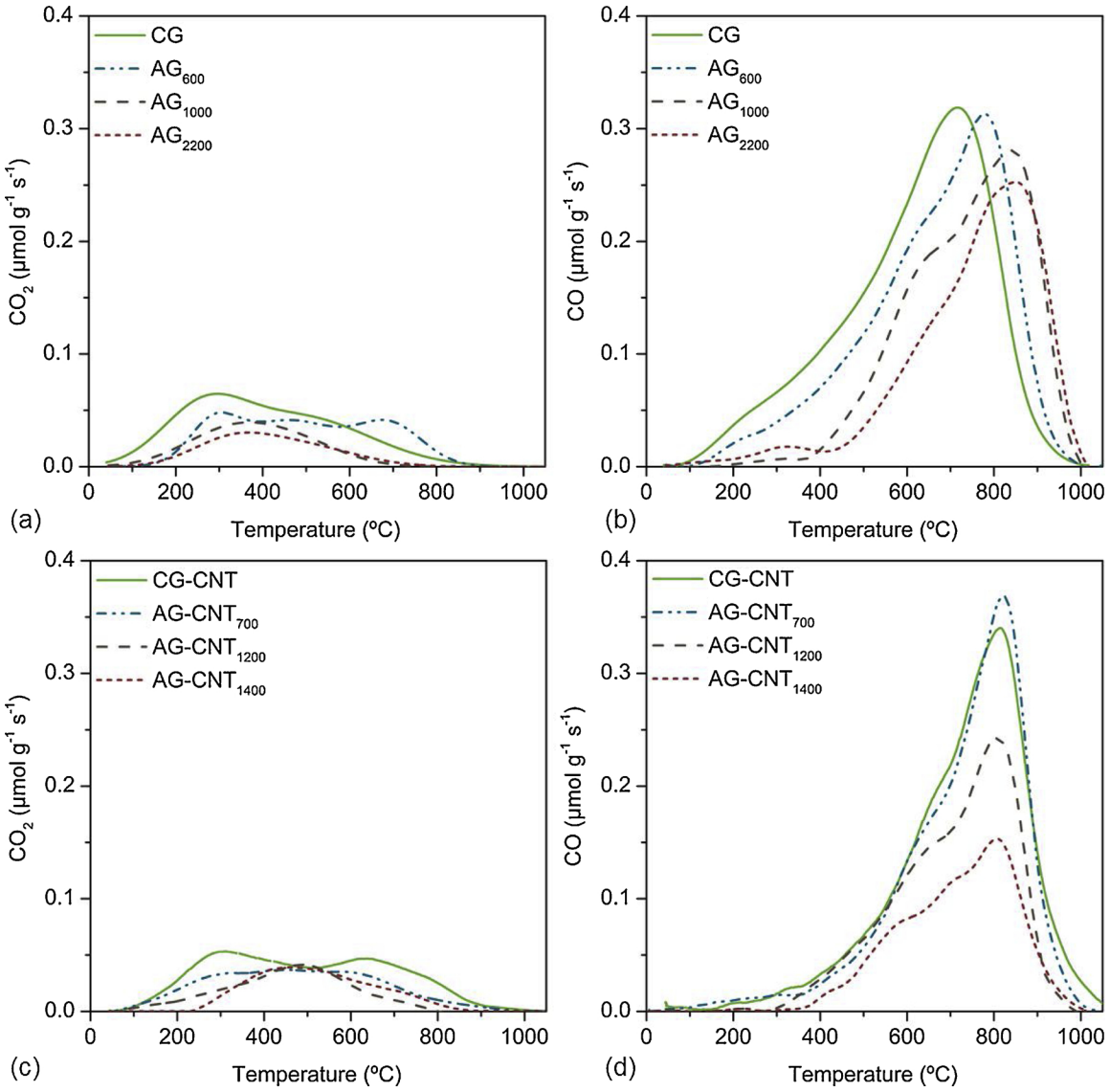

Fig. 2. CO_2 and CO TPD profiles of the supports prepared from glucose-derived carbons (a) and (b) and from glucose-derived/CNT hybrids (c) and (d).

chemical structure due to the presence of CNT during the polymerization. This result is in line with the above-mentioned hypothesis about the interaction of CNT with the oxygen groups of the glucose structure during the hydrothermal carbonization [41]. Moreover, in the CO_2 profile, the contribution of the carboxylic acids and carboxylic anhydrides decreases in comparison with the contributions of sample CG, while the amount of lactones increases. In the CO profile the amount of carboxylic anhydrides and phenols decreases, while the contribution of the carbonyl-quinone groups increases.

These results suggest that the hybrid sample has a higher contribution of basic functional groups on its surface, which is in agreement with the lower value of phenol/carbonyl-quinone ratio shown in Table 4 (0.61 and 0.40 for samples CG and CG-CNT, respectively). Alike in activated samples without CNT, some differences in the oxygen surface functionalization of the hybrid activated samples are also observed due to activation conditions (Fig. 2c and d). The contribution of the peaks in the CO_2 and CO profiles decreases by increasing the temperature and time of activation. However, no noticeable difference in the temperatures at which the peaks are released is observed, indicating similar thermal stability for all the carbon structures, probably due to the presence of CNT. In addition, the phenol/carbonyl-quinone ratio of the hybrid materials increases with the degree of activation (from 0.41 to 0.81, Table 4), suggesting the presence of more acid functionalities due to the reaction with the activating agent. These results demonstrate that the effect of activation depends to a large extent on the presence of CNT into the initial structure of the samples. In fact, a comparison between the CO profile of samples with and without CNT treated under the same conditions also indicates differences in the surface functionalities (Fig. 2b and d). The CO profile for hybrid samples in the region involving phenols and carbonyl-quinone groups is narrower than that shown for glucose-derived carbons, besides being more centered at higher temperatures, attributed to the carbonyl-quinone group. These results indicate a smaller contribution of phenols for the hybrid materials (Table S2). Accordingly, a more basic surface is expected due to the addition of CNT. These results are corroborated by the phenol/carbonyl-quinone ratio, which is higher for samples without CNT, with the exception of sample AG-CNT_{1400}, which shows a higher acidic character. The unexpected surface functionalities of sample AG-CNT_{1400} can be explained by the reactivity of the sample towards CO_2. At the beginning of the activation process, the activation agent (CO_2) reacts with the amorphous glucose particles giving rise to a material with high microporosity (Table 3). The amount of glucose particles decreases as the time of activation increases, and CO_2 also starts to react with the CNT, oxidizing its innermost parts, i.e., the inner wall of the

carbon nanotubes [42]. These new oxygen functionalities are stable enough to remain into the structure in spite of the high temperature used during activation.

3.2. Characterization of catalysts

N_2 adsorption-desorption isotherms of glucose-derived carbon and hybrid catalysts were performed to evaluate any possible modification on the textural properties due to the method used for the preparation of the catalysts: incipient wetness impregnation. The isotherms obtained and the most important textural parameters are shown in Figure S3 and Table S3 in the supporting information. The shape of the isotherms of all catalysts is maintained with respect to their counterpart supports, even though microporosity decreases due to the presence of the metal. The decrease in the surface area may be attributed to the blocking of micropores by small metal nanoparticles. Moreover, the loss of microporosity increases with the degree of activation. Samples with higher surface area also exhibit wider pore sizes that favor the diffusion of the solution containing the metal through the innermost part of the porous structure (pore size distribution of all catalysts are shown in Fig. 3). Therefore, the metal is deposited inside the porous structure blocking a higher proportion of micropores. The external surface areas of the catalysts follow the same trend as their counterpart supports and, like the BET surface area, the values of S_{ext} decrease by the incorporation of the metal (Table S3).

The morphology of two catalysts with similar microporosity (Ru/CG and Ru/AG_{600}) was examined by scanning electron microscopy (SEM) and transmission electron microscopy (TEM). Both samples are composed of spheres of 300–400 nm, which is a typical morphology of hydrothermal carbons (Fig. 4a and b). In addition, Ru particles were detected all over the surface of the spheres, as shown in TEM images (Fig. 4c and d). The Ru nanoparticles are well dispersed over the entire surface of the carbon materials with an average size of 1.7–1.8 nm (particle size distribution is shown in Figure S4). To explore deeper into the surface of the samples, the surface elemental compositions of these two catalysts (Ru/CG and Ru/AG_{600}) were also analyzed by XPS.

The main signal of ruthenium appears inside the C 1s region, which may hinder the metal characterization. Therefore, the surface elemental composition of the carbonized (CG) and the activated (AG_{600}) support was also analyzed to clearly distinguish the contributions of the support from those of the metal. The XPS survey spectra of the CG and AG_{600} samples are presented in Figure S5, from which it can be confirmed that only carbon and oxygen are present in the samples. The high-resolution XPS spectra in the C 1s region was deconvoluted into five peaks (Fig. 5) attributed to [43]: i) sp^2-hybridized carbon atoms (284.6 eV), ii) single bonded C—O groups in phenols and ethers (286.1 ± 0.1 eV), iii) double bonded C═O groups in ketones and quinones (287.2 ± 0.2 eV), iv) carbon-oxygen groups in carboxylic acids and ester species (288.8 ± 0.3 eV) and v) the characteristic π-π* shake-up satellite peak from the sp^2-hybridized carbon atoms in aromatic compounds (290.6 ± 0.2 eV). The proportion of phenols and carbonyl-quinones is slightly lower in the activated sample, while the contribution of the peak attributed to the carboxylic acids decreases. These results are in agreement with those previously observed by the TPD measurements already discussed. The XPS survey spectra of the Ru/CG and Ru/AG_{600} catalysts are also presented in Figure S5. In addition to carbon and oxygen, the peak of ruthenium is also observed, while the Cl 2p (200.0 eV) signal was not detected in the survey spectrum, indicating the complete decomposition of the $RuCl_3$ precursor.

The chemical state of ruthenium over the surface of the catalysts was evaluated by analyzing the less intense Ru 3p signal and the main Ru 3d signal in the C1 s region. The XPS spectra for Ru 3p region of the prepared catalysts are shown in Figure S6. The catalysts showed two strong peaks at 462.5 ± 0.1 eV and 484.7 ± 0.1 eV attributed to Ru 3p3/2 and Ru 3p1/2 respectively. The binding energy obtained for Ru 3p3/2 is similar to those previously reported for Ru metallic

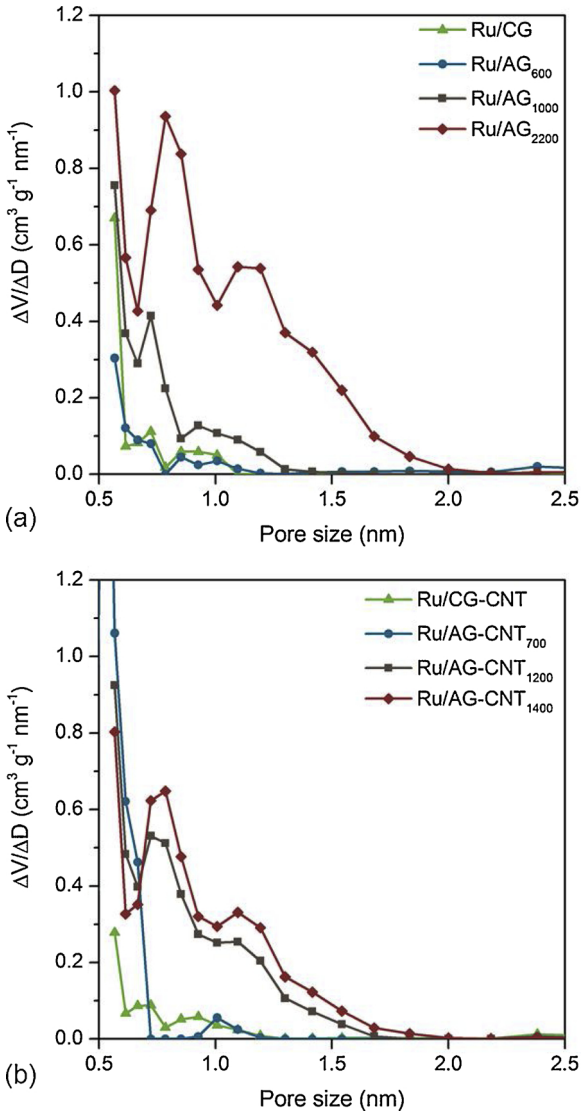

Fig. 3. Pore size distributions of the supported Ru catalysts on glucose-derived (a) and hybrid catalysts (b).

nanoparticles supported on carbon materials (462.2 eV) [23,44]. It should be noted that these binding energies are slightly shifted to higher values in comparison with the theoretical value (461.2 eV), probably due to the stronger interaction between metallic Ru particles and the glucose-derived carbon support [23]. The same trend is observed in the XPS spectra in the C 1s region (Fig. 5c and d), in which the main Ru 3d signal (281.1 ± 0.1 eV) also appears slightly shifted from the theoretical value (280.5 eV) [45]. This peak also shows the corresponding spin-orbit splitting at + 4.17 eV.

It should be highlighted that, from the results above, it could also be considered that ruthenium is in its oxidized form (RuO_2). In that case, ruthenium should also appear in the oxygen XPS spectra. The deconvolution of the XPS spectra in the O 1s region shows the same three peaks for supports and catalysts (Figure S7). These peaks are attributed to: i) carbonyl oxygen (peak at 530.8 eV ± 0.2 eV), C—O groups in phenols and ethers (peak at 532.2 ± 0.2 eV) and oxygen atoms in carboxylic acids and esters species (peak at 533.5 ± 0.3 eV). The peak at 529.5–530.1 eV ascribed to RuO_2 is in the same range than carbonyl oxygen. The contribution of carbonyl oxygen in the catalysts is higher than that observed for the supports, which could lead to the conclusion that ruthenium is in its oxidized form. However, the trends of the oxygen functionalities in the O 1s region are in agreement with those

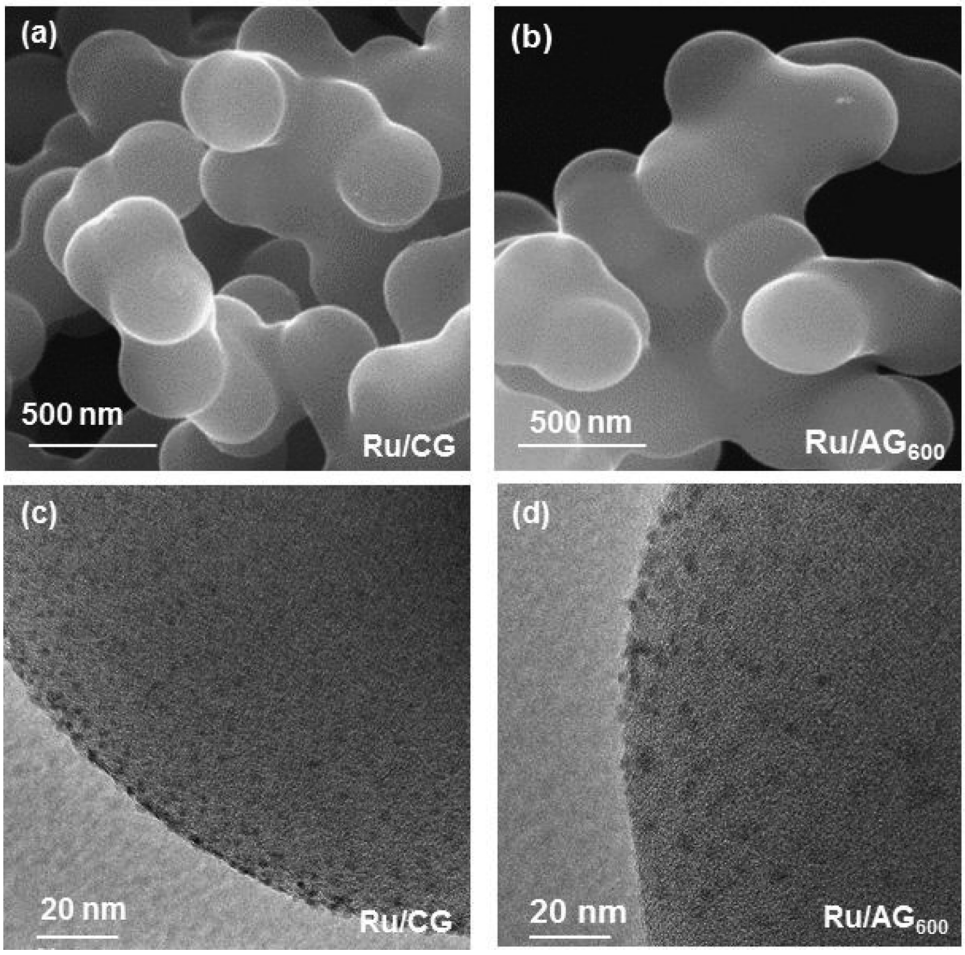

Fig. 4. SEM (a and b) and TEM (c and d) images of the ruthenium supported on glucose-derived carbons catalysts prepared by carbonization and physical activation.

shown in the C 1s region, i.e., the contribution of the carbonyl oxygen increases, while the contribution of carboxylic acids decreases after the incorporation of the metal. This result suggests that the increase in carbonyl oxygen region is not due to the presence of RuO_2. In addition, these results are confirmed by temperature programmed reduction (TPR) analysis of the supports and the catalysts before and after impregnation (Figure S8). Therefore, it is clear that all ruthenium is in its metallic state and the slight deviation of the binding energies in Ru 3p and Ru 3d signal is probably due to its strong interaction with the carbon support.

3.3. Catalytic performance in cellulose conversion

The catalytic reaction was first performed using carbon supports without the addition of the metal phase (CG and CG-CNT). It was observed that about 92–100 % of ball-milled cellulose was converted after 5 h of reaction. However, very low yields of hexitols (glucose, sorbitol and glycerol) were obtained (Figure S9). The prepared carbon supported Ru catalysts were then employed for the hydrolytic hydrogenation of cellulose. The effect of the textural and chemical properties of the carbon supports was evaluated by keeping similar theoretical Ru loading (0.4 wt. %) and reaction conditions. Fig. 6 shows the catalytic performance of the studied catalysts for cellulose conversion. The reference material Ru/CNT has also been added in Fig. 6b for comparison (data of this sample taken from reference [26]).

At the beginning of the reaction, the conversion of cellulose is higher than zero (about 20%) since $t = 0$ min corresponds to the introduction of hydrogen into the reactor. Before introducing hydrogen, the reactor is previously heated to 205 °C under nitrogen. This step lasts about 100 min, which is time enough to start cellulose conversion, as shown in Fig. 6. Once hydrogen is introduced into the reactor, the catalyst supported on CG presented a higher initial conversion rate than the catalyst supported on the activated sample with similar surface area (Ru/AG_{600}). Sample Ru/CG exhibits a slightly higher amount of acidic surface functionalities, which favors the hydrolysis of cellulose into glucose, and hence, a more pronounced conversion is observed during the first hour of reaction. However, sample Ru/AG_{2200} exhibits the highest conversion rate of all activated samples despite having a less acidic surface. This sample exhibits the broadest pore size, which could favor a faster diffusion of the reagents, and hence, the conversion rate. This result suggests the important role of microporosity on the conversion of cellulose. In fact, it can be inferred from Fig. 6a that, for a given reaction time, the conversion decreases with the surface area of the catalysts. Notwithstanding, all catalysts supported on activated samples showed complete conversion of cellulose after 3 h of reaction, indicating their high performance for cellulose degradation.

Catalysts containing CNT exhibit a quite similar initial conversion rate (for the first half hour), which is also comparable to that obtained for Ru supported on CNT. Nevertheless, the conversion rate achieved for all hybrid catalysts is much higher than that obtained for the Ru catalyst supported on CNT (reference material). A comparison between Ru supported on hybrid materials reveals that, unlike in Ru supported on activated samples, the trend of the conversion for high values of reaction time does not seem to be directly related to the textural properties of the catalysts. Although sample $Ru/AG\text{-}CNT_{1200}$ exhibits higher conversion rate than sample $Ru/AG\text{-}CNT_{700}$, further activation (sample $Ru/AG\text{-}CNT_{1400}$) results in a decrease of the conversion, suggesting that the conversion of cellulose is related to both the textural

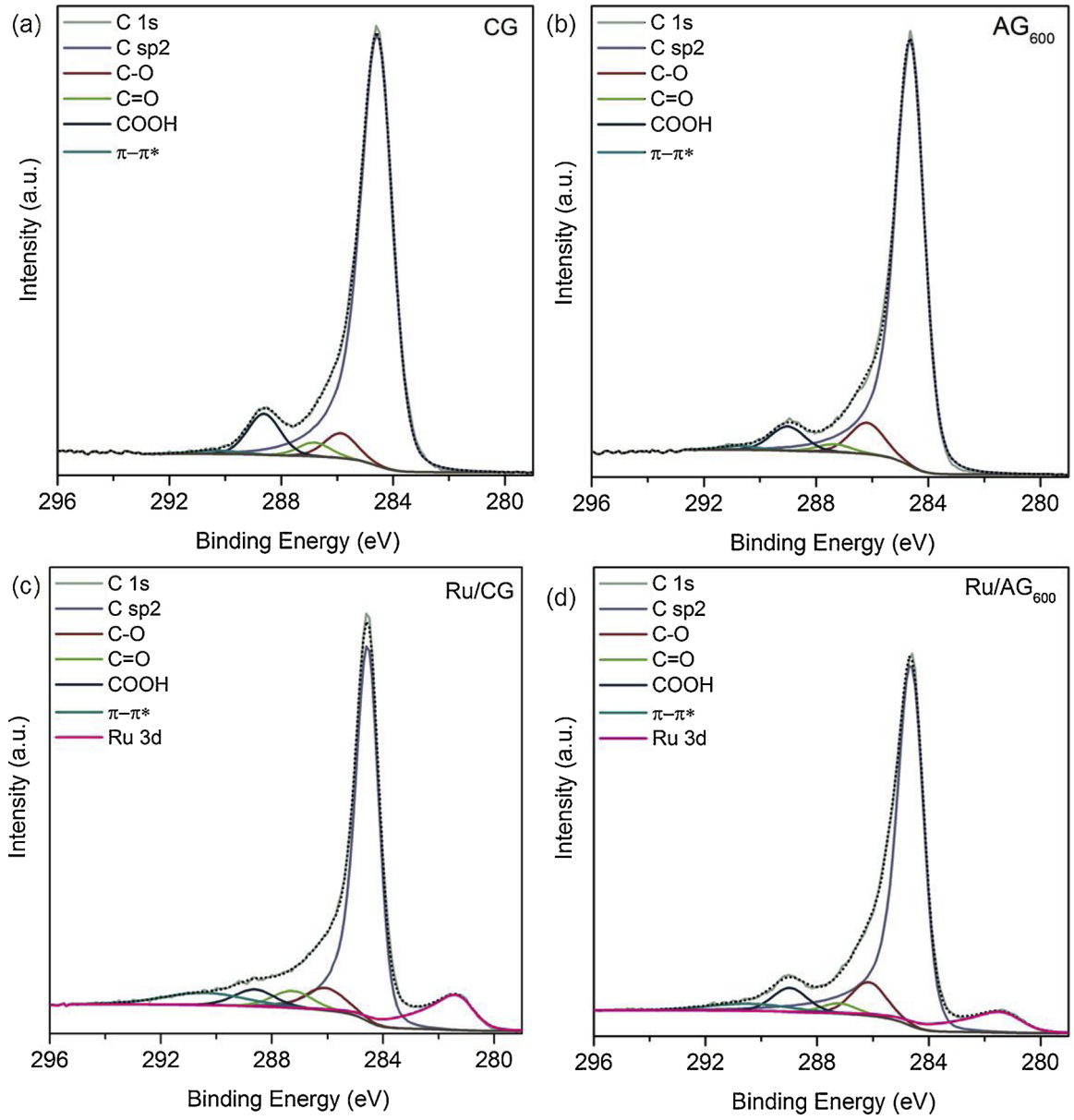

Fig. 5. XPS spectra of C 1d for sample CG (a), AG_{600} (b), Ru/CG (c) and Ru/AG_{600} (d).

and chemical properties of the catalysts. Even so, all hybrid catalysts showed complete conversion of cellulose after 3 h of reaction, indicating their high performance for cellulose degradation.

3.4. Influence of catalyst properties on the production of sorbitol

The direct conversion of cellulose results in different polyols such as sorbitol, ethylene glycol, propylene glycol, together with glucose, glycerol and formic acid (Table 5). The scheme of the possible routes to produce each chemical product is shown in Fig. 7. Sorbitol was detected as the main product in the reaction mixture, while the yield of the listed by-products did not exceed 12% each, as shown in Table 5. Besides the six main identified products shown in Table 5, the production of other compounds such as cellobiose, mannose, fructose, xylitol, erythritol, glycolaldehyde, levulinic acid, furfural and 5-hydroxymethylfurfural were also analyzed, although none of them were detected.

Differences in the catalytic selectivity of each catalyst are observed, highlighting that the properties of the supports have a strong influence on the production of sorbitol directly from cellulose. The catalyst prepared on carbonized glucose (sample Ru/CG) resulted in a yield of sorbitol lower than that published for Ru supported on other types of carbon materials, such as CNT (50.9% sorbitol yield after 5 h [26]). However, the activation of the sample led to an increase of the yield of sorbitol of up to 40% (from 33.1 to 55.3%), namely in the order of $Ru/AG_{600} < Ru/AG_{1000} < Ru/AG_{2200}$, along with a decrease in the yield of formic acid. To evaluate these differences in the catalytic selectivity, the values of Ru loading were measured by ICP. A value of 0.48 wt. % was obtained for sample Ru/CG, while for all activated samples a loading of 0.44-0.46 wt.% was determined. Accordingly, the trends shown in Table 5 can be ascribed to two different factors: i) higher surface area, and ii) lower acidity of the surface. In order to evaluate the effect of these factors, the evolution of the production of sorbitol with reaction time over all the supported Ru catalysts is shown in Fig. 8.

The production of sorbitol increases with the surface area of the supports (Fig. 8a). The access to the metal is faster in the sample with a more developed porous structure (sample Ru/AG_{2200}), favoring the hydrogenation of glucose into sorbitol. Moreover, the less acidic character of the surface of these catalysts suppresses the isomerization of glucose to fructose, limiting the further conversion to 5-HMF and subsequently formic acid (route 1 in Fig. 7). From Fig. 8a it can also be

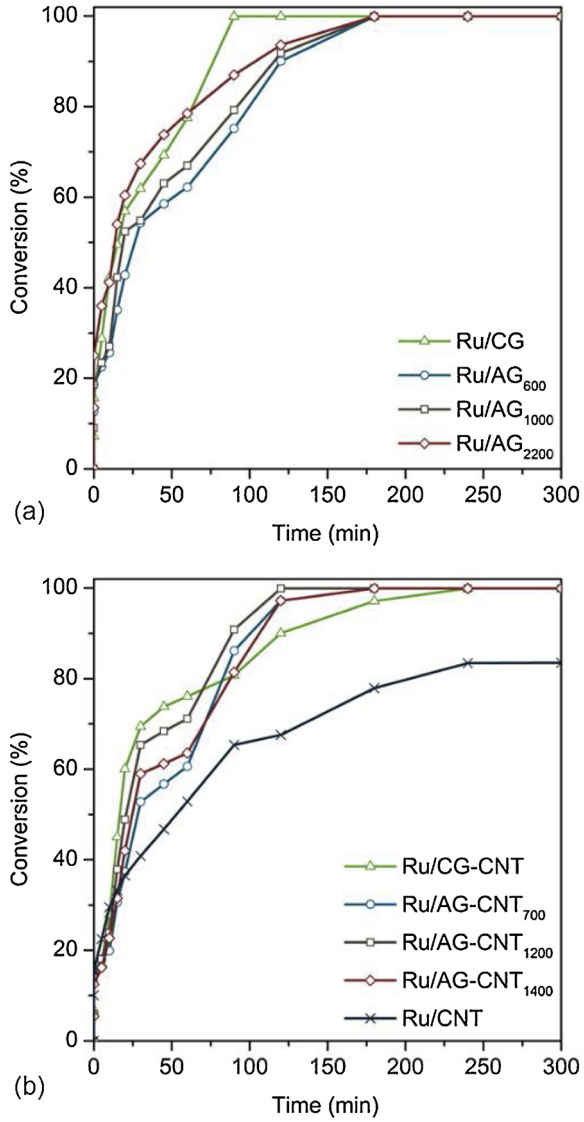

Fig. 6. Evolution of cellulose conversion with the reaction time over the Ru catalysts supported on glucose-derived carbons prepared in the absence (a) and presence (b) of carbon nanotubes. Reaction conditions: ball-milled cellulose (0.75 g), water (300 mL), catalyst (0.30 g), 205 °C, 50 bar H_2, 150 rpm.

Table 5
Catalytic results of cellulose conversion and products distribution*.

Entry	Catalyst	X (%)	Yields** (%)						
			SOR	EG	PG	GLU	GLY	FORM	Others
1	Ru/CG	100	33.1	5.3	6.3	0.0	4.0	9.3	42.0
2	Ru/AG_{600}	100	45.1	2.9	5.0	4.3	0.0	9.5	33.2
3	Ru/AG_{1000}	100	52.8	8.6	5.7	4.4	4.5	6.4	17.6
4	Ru/AG_{2200}	100	55.3	0.7	2.6	4.5	3.6	5.1	28.2
5	Ru/CG-CNT	100	40.4	2.4	0.0	0.0	1.8	12.1	43.3
6	$Ru/AG\text{-}CNT_{700}$	100	52.5	1.0	3.1	0.0	0.0	10.8	32.6
7	$Ru/AG\text{-}CNT_{1200}$	100	60.4	0.6	3.3	0.0	4.1	4.0	27.6
8	$Ru/AG\text{-}CNT_{1400}$	100	20.9	2.3	0.0	0.0	6.6	0.0	70.2

* Reaction conditions: 750 mg ball-milled cellulose, 300 mg catalyst, 300 mL H_2O, 205 °C, 50 bar H_2, 150 rpm, 5 h.
** SOR: sorbitol; EG: ethylene glycol; PG: propylene glycol; GLU: glucose; GLY: glycerol; FORM: formic acid.

inferred that the initial production of sorbitol is quite similar for samples Ru/CG and Ru/AG_{600}, but Ru/AG_{600} gives rise to higher yields with reaction time. Ru/CG and Ru/AG_{600} catalysts have similar porosity and morphology (see Section 3.2), and contain similar Ru loadings (0.48 and 0.44 wt.% Ru, respectively). Therefore, the higher yields attained using the activated support can be related to the differences in the surface functionalities. The acidity of the catalyst Ru/AG_{600} is lower than that of Ru/CG, avoiding further hydrogenolysis of sorbitol into ethylene glycol, propylene glycol and glycerol (route 2 in Fig. 7) [32]; hence, higher yield of sorbitol is obtained. Experimental data presented in Fig. 8a provide further information about the behavior of the Ru catalysts supported on activated materials. The yield of sorbitol exhibited a continuous increase by increasing the reaction time up to 3 h. However, further prolongation of the reaction time results in a slight drop of the yield of sorbitol for sample Ru/AG_{2200}, indicating that sorbitol could be starting to undergo further hydrogenation/hydrogenolysis to produce other polyols or even gaseous products.

The presence of CNT in the glucose structure had a positive effect on the yield of sorbitol, which increased from 33.1% using Ru/CG to 40.4% using Ru/CG-CNT, accompanied by the decrease of the yields of EG, PG and GLY (Table 5: entries 1 and 5). This improvement may be due to the higher amount of Ru in sample Ru/CG-CNT (0.63 wt.%). However, this value is still below that previously obtained using Ru supported on carbon nanotubes (50.9% sorbitol yield after 5 h [26]) and those achieved for supports obtained by the activation of glucose-derived carbons (45.1–55.3 % sorbitol yields after 5 h, Table 5: entries 1–4). Accordingly, the evolution of the yield of sorbitol with reaction time by using the set of catalysts prepared on activated glucose/CNT hybrids was investigated. The results obtained are plotted in Fig. 8b. As in Ru supported on glucose-derived carbons without CNT, the yield of sorbitol achieved was higher using the activated material ($Ru/AG\text{-}CNT_{700}$) than the carbonized sample (Ru/CG-CNT), despite containing similar Ru loadings (0.63 and 0.62 wt.% Ru, respectively). Moreover, it should be noticed that the $Ru/AG\text{-}CNT_{700}$ catalyst allowed to match the yield of sorbitol previously published using Ru/CNT, and that this value is surpassed for $Ru/AG\text{-}CNT_{1200}$ catalyst, probably due to its higher surface area. In fact, the highest yield of sorbitol was achieved over the $Ru/AG\text{-}CNT_{1200}$ catalyst within 3 h of reaction (64.1%) and, even though the yield underwent a small decrease from 64.1 to 60.4% with further increase of the reaction time to 5 h, this value is still one of the highest values published to date for the production of sorbitol using carbon supported catalysts. Similar values have been published using carbon supported catalysts such as carbon nanotubes, biomass-derived carbons, carbon nanofibers, and activated carbons [12,46–48]. However, the reaction time used in those studies was more than 4 times higher the time used in the present study.

It is also noticeable from Fig. 8b that the yield of sorbitol is not only associated to the specific surface area, as can be seen by comparing the results obtained for catalyst $Ru/AG\text{-}CNT_{1200}$ and $Ru/AG\text{-}CNT_{1400}$. This phenomenon corroborates the hypothesis related to the effect of the chemical surface functionalities of the supports on the production of sorbitol. Sample $AG\text{-}CNT_{1400}$ exhibits a CO/CO_2 ratio similar to that of CG/CNT, but twice the phenol/carbonyl-quinone ratio (Table 4), suggesting that the more acidic functionalities do not favor the production of sorbitol. In order to confirm such hypothesis, a ruthenium catalyst prepared on an oxidized support (CG_{HNO3}) was also tested for the one-pot reaction (all information related to the preparation and characterization of this sample can be found in the supporting information). The use of CG_{HNO3} as Ru support induced a higher initial conversion rate than the catalyst supported on the pristine support (sample CG), as shown in Figure S11a in the supporting information. However, the conversion rate sharply decreases after 5 min of reaction. The catalyst supported on CG yields a complete conversion of cellulose in 90 min of reaction, whereas, for the same reaction time, the acidified sample only allowed 60% conversion and about 5 h are needed to attain complete conversion of cellulose. This result can be attributed to the higher

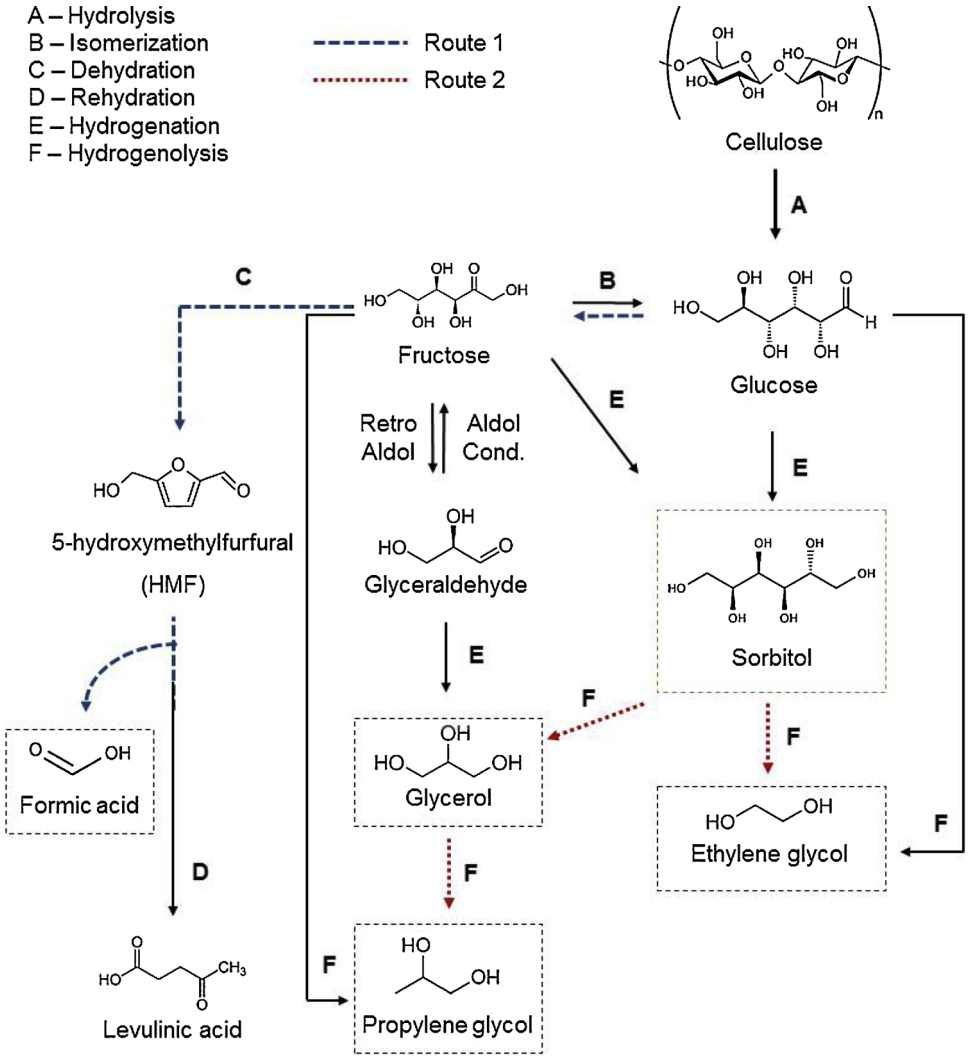

Fig. 7. Scheme for the conversion of cellulose into added-value chemical products.

acidity of Ru/CG_{HNO3} compared to Ru/CG, as evidenced by TPD analysis (Figure S10). The same trend is observed for the yield of sorbitol that significantly decreased from 33.1 to 14.1% (Figure S11b). In this case, the acid surface functionalities of sample CG_{HNO3} favored the formation of EG and formic acid, which yields increased from 6.3 to 10.5% and from 9.3 to 12.3%, respectively. These results demonstrate that the introduction of acidic oxygen functionalities is detrimental for sorbitol production. Accordingly, supports with high surface area and low acidic oxygen functionalities are desirable for the direct conversion of cellulose into sorbitol. In the case of biomass-derived carbons, the microporosity can be easily tailored and the amount of oxygen can be further reduced by the introduction of a small amount of carbon nanotubes yielding a sorbitol production higher than that obtained using only CNT as support.

3.5. Stability of the catalysts

From an environmental and industrial point of view, the stability of the catalyst is very important considering continuous production processes. Therefore, the recyclability of the most efficient catalyst (Ru/AG-CNT_{1200}) was examined. Fig. 9 pinpoints that Ru/AG-CNT_{1200} could be successfully recycled for at least 4 runs. No essential change was observed in the conversion of cellulose (100% in all runs) nor in the yield of sorbitol. After the one-pot reaction (5 h), the yield of sorbitol ranges from 60.4 to 64.7% over the repeated runs (Fig. 9). However, as the reaction was conducted at a temperature at which water solvent become acidic and the ruthenium itself may suffer oxidation, the surface elemental composition of the catalyst Ru/AG-CNT_{1200} before and after the reaction was analyzed by XPS. The evaluation of the less intense Ru 3p signal and the main Ru 3d signal in the C1s region shows that the state of the metal has not changed during the reaction. The deconvolution of the regions C 1s, O 1s and Ru 3p (Figure S12 and S13) shows the same peaks previously observed for the catalysts Ru/CG and Ru/AG_{600}, which suggest that ruthenium continues in its metallic state. However, some differences in the contribution of each component are observed, particularly for oxygen. The amount of oxygen detected on the surface of the used catalyst is higher than that observed for the fresh catalyst. In addition, the contribution of carbonyl oxygen in the O 1s region (peak at 530.8 eV ± 0.2 eV) has increased significantly, while the relative contribution of the C—O groups in phenols and ethers (peak at 532.2 ± 0.2 eV) and oxygen atoms in carboxylic acids and esters (peak at 533.5 ± 0.3 eV) has decreased. The trends of the oxygen functionalities in the O 1s region are in agreement with those shown in the C 1s region, which suggest that oxygen has been incorporated into the surface of the support and it is not linked to the metal (also corroborated by the peaks in the Ru 3p region). Besides, it seems that the reaction conditions favor the incorporation of basic oxygen functionalities, which could explain the successful recycling of the catalyst. Therefore, these results demonstrate that the synthesized catalyst is stable and reusable at least up to four cycles under the conditions

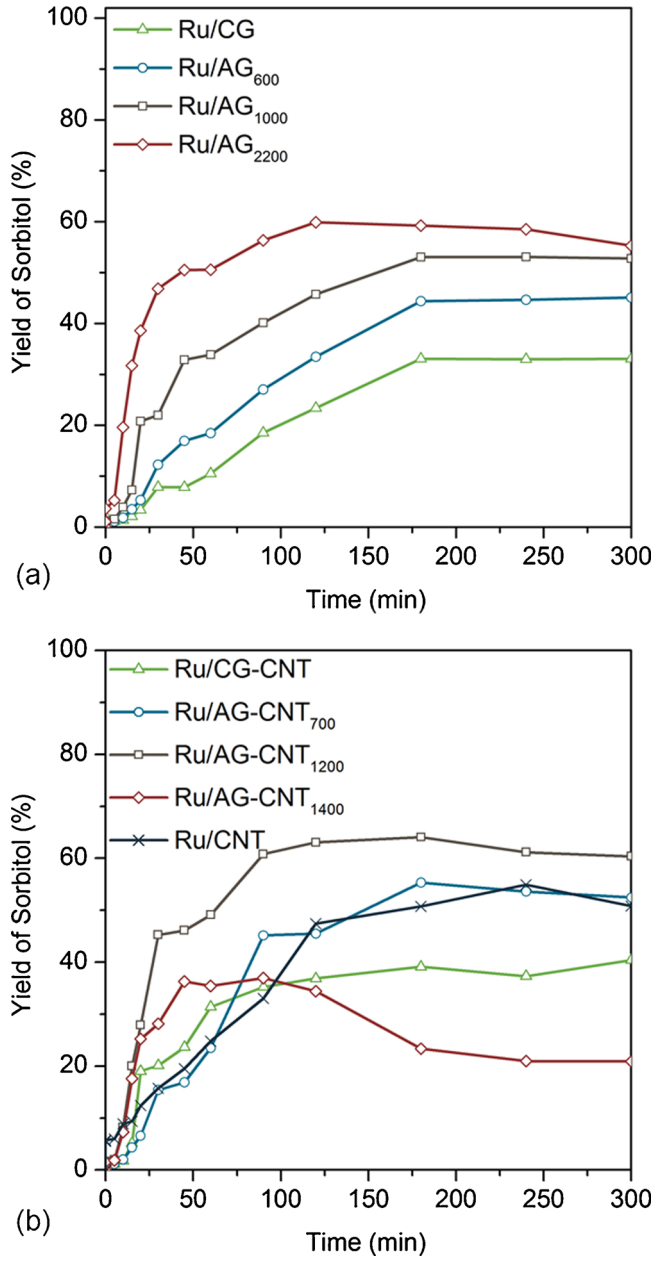

Fig. 8. Evolution of the yield of sorbitol with reaction time over the Ru catalysts supported on glucose-derived carbons prepared in the absence (a) and presence (b) of carbon nanotubes. Reaction conditions: ball-milled cellulose (0.75 g), water (300 mL), catalyst (0.30 g), 205 °C, 50 bar H_2, 150 rpm.

studied. Moreover, the values obtained surpassed that obtained using carbon nanotube supported Ru catalysts under the same conditions, so AG-CNT_{1200} is herein presented as a cheaper and sustainable replacement for CNT as catalytic support.

4. Conclusions

The hydrothermal methodology provides a simple and effective method to obtain catalysts with tailored textural and chemical properties. Regardless of the presence of CNT, an increase in temperature and time of activation results in materials with higher microporosity and lower oxygen content. In addition, the incorporation of CNT during the polymerization of glucose results in supports with a more stable chemical structure and more basic surface functionalities, which favors the direct conversion of cellulose to sorbitol. Indeed, the following general conclusions were withdrawn from the results obtained: i) the yield of sorbitol increased with the specific surface area of the carbon supports and ii) the basic functional groups on the surface of the catalysts prevent further hydrogenolysis of sorbitol into polyols. Thus, the appropriate activation conditions and the addition of CNT during the polymerization of glucose led to the most efficient catalyst for the conversion of cellulose. A yield of 64% of sorbitol was achieved after 3 h of reaction even after four reaction cycles, which is the highest value reported for the direct conversion of cellulose to sorbitol over carbon supports using a nominal amount of metal as low as 0.4 wt.%. Thus, glucose-derived carbons stand as good and sustainable alternative catalyst supports for the efficient production of sorbitol, which in addition allows valorizing biomass for both the preparation of the catalyst and as the main raw material of the reaction.

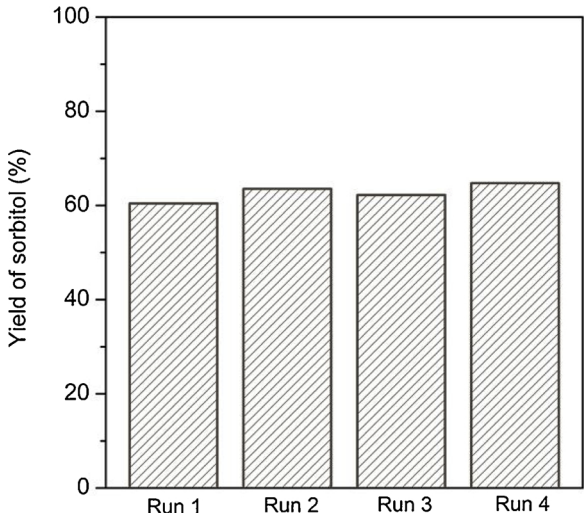

Fig. 9. Recycling test of the Ru/AG-CNT_{1200} catalyst on sorbitol yield after 5 h of reaction. Reaction conditions: ball-milled cellulose (0.75 g), water (300 mL), Ru/AG-CNT_{1200} (0.30 g), 205 °C, 50 bar H_2, 150 rpm, 5 h.

Acknowledgments

This work was financially supported by Project "AIProcMat@N2020 - Advanced Industrial Processes and Materials for a Sustainable Northern Region of Portugal 2020", with the reference NORTE-01-0145-FEDER-000006, supported by Norte Portugal Regional Operational Programme (NORTE 2020), under the Portugal 2020 Partnership Agreement, through the European Regional Development Fund (ERDF); Associate Laboratory LSRE-LCM - UID/EQU/50020/2019 - funded by National funds through FCT/MCTES (PIDDAC); project "UniRCell", with the reference POCI-01-0145-FEDER-016422. The authors are indebted to Rui Rocha and to Dr. Carlos M. Sá (CEMUP) for assistance with SEM and XPS analyses, respectively.

Appendix A. Supplementary data

Supplementary material related to this article can be found, in the online version, at doi:https://doi.org/10.1016/j.apcatb.2019.117826.

References

[1] M. Grilc, B. Likozar, Levulinic acid hydrodeoxygenation, decarboxylation and oligmerization over NiMo/Al2O3 catalyst to bio-based value-added chemicals: Modelling of mass transfer, thermodynamics and micro-kinetics, Chem. Eng. J. 330 (2017) 383–397.
[2] B. Hočevar, M. Grilc, M. Huš, B. Likozar, Mechanism, ab initio calculations and microkinetics of hydrogenation, hydrodeoxygenation, double bond migration and cis–trans isomerisation during hydrotreatment of C6 secondary alcohol species and ketones, Appl. Catal. B 218 (2017) 147–162.
[3] B. Hočevar, M. Grilc, M. Huš, B. Likozar, Mechanism, ab initio calculations and

microkinetics of straight-chain alcohol, ether, ester, aldehyde and carboxylic acid hydrodeoxygenation over Ni-Mo catalyst, Chem. Eng. J. 359 (2019) 1339–1351.
[4] M. Yabushita, H. Kobayashi, A. Fukuoka, Catalytic transformation of cellulose into platform chemicals, Appl. Catal. B 145 (2014) 1–9.
[5] M. Besson, P. Gallezot, C. Pinel, Conversion of biomass into chemicals over metal catalysts, Chem. Rev. (Washington, DC, U.S.) 114 (2014) 1827–1870.
[6] B. Zada, M. Chen, C. Chen, L. Yan, Q. Xu, W. Li, Q. Guo, Y. Fu, Recent advances in catalytic production of sugar alcohols and their applications, Sci. China Chem. 60 (2017) 853–869.
[7] A. Shrotri, H. Kobayashi, A. Fukuoka, Cellulose depolymerization over heterogeneous catalysts, Acc. Chem. Res. 51 (2018) 761–768.
[8] J. Zhang, J. Li, S. Wu, Y. Liu, Advances in the catalytic production and utilization of sorbitol, Ind. Eng. Chem. Res. 52 (2013) 11799–11815.
[9] K. Gao, J.Y. Xin, D.X. Yan, H.X. Dong, Q. Zhou, X.M. Lu, S.J. Zhang, Direct conversion of cellulose to sorbitol via an enhanced pretreatment with ionic liquids, J. Chem. Technol. Biotechnol. 93 (2018) 2617–2624.
[10] L.S. Ribeiro, J.J.M. Órfão, M.F.R. Pereira, Enhanced direct production of sorbitol by cellulose ball-milling, Green Chem. 17 (2015) 2973–2980.
[11] J.W. Han, H. Lee, Direct conversion of cellulose into sorbitol using dual-functionalized catalysts in neutral aqueous solution, Catal. Commun. 19 (2012) 115–118.
[12] W. Deng, X. Tan, W. Fang, Q. Zhang, Y. Wang, Conversion of cellulose into sorbitol over carbon nanotube-supported ruthenium catalyst, Catal. Lett. 133 (2009) 167.
[13] B. Zhang, X. Li, Q. Wu, C. Zhang, Y. Yu, M. Lan, X. Wei, Z. Ying, T. Liu, G. Liang, F. Zhao, Synthesis of Ni/mesoporous ZSM-5 for direct catalytic conversion of cellulose to hexitols: Modulating the pore structure and acidic sites: Via a nanocrystalline cellulose template, Green Chem. 18 (2016) 3315–3323.
[14] P. Yang, H. Kobayashi, K. Hara, A. Fukuoka, Phase change of nickel phosphide catalysts in the conversion of cellulose into sorbitol, ChemSusChem 5 (2012) 920–926.
[15] S. Van de Vyver, J. Geboers, M. Dusselier, H. Schepers, T. Vosch, L. Zhang, G. Van Tendeloo, P.A. Jacobs, B.F. Sels, Selective bifunctional catalytic conversion of cellulose over reshaped Ni particles at the tip of carbon nanofibers, ChemSusChem 3 (2010) 698–701.
[16] A. Negoi, K. Triantafyllidis, V.I. Parvulescu, S.M. Coman, The hydrolytic hydrogenation of cellulose to sorbitol over M (Ru, Ir, Pd, Rh)-BEA-zeolite catalysts, Catal. Today 223 (2014) 122–128.
[17] X. Zhang, L.J. Durndell, M.A. Isaacs, C.M.A. Parlett, A.F. Lee, K. Wilson, Platinum-catalyzed aqueous-phase hydrogenation of d-glucose to d-sorbitol, ACS Catal. 6 (2016) 7409–7417.
[18] L.S. Ribeiro, J.J.M. Órfão, M.F.R. Pereira, Comparative study of different catalysts for the direct conversion of cellulose to sorbitol, Green Process. Synth. 4 (2015) 71–78.
[19] A. Romero, E. Alonso, Á. Sastre, A. Nieto-Márquez, Conversion of biomass into sorbitol: cellulose hydrolysis on MCM-48 and d-Glucose hydrogenation on Ru/MCM-48, Microporous Mesoporous Mater. 224 (2016) 1–8.
[20] W. Zhu, H. Yang, J. Chen, C. Chen, L. Guo, H. Gan, X. Zhao, Z. Hou, Efficient hydrogenolysis of cellulose into sorbitol catalyzed by a bifunctional catalyst, Green Chem. 16 (2014) 1534–1542.
[21] D.K. Mishra, A.A. Dabbawala, J.J. Park, S.H. Jhung, J. Hwang, Selective hydrogenation of d-glucose to d-sorbitol over HY zeolite supported ruthenium nanoparticles catalysts, Catal. Today 232 (2014) 99–107.
[22] J. Xi, Y. Zhang, Q. Xia, X. Liu, J. Ren, G. Lu, Y. Wang, Direct conversion of cellulose into sorbitol with high yield by a novel mesoporous niobium phosphate supported Ruthenium bifunctional catalyst, Appl. Catal. A Gen. 459 (2013) 52–58.
[23] A.A. Dabbawala, D.K. Mishra, J. Hwang, Selective hydrogenation of D-glucose using amine functionalized nanoporous polymer supported Ru nanoparticles based catalyst, Catal. Today 265 (2016) 163–173.
[24] L.S. Ribeiro, J.J. Delgado, J.J.M. Órfão, M.F.R. Pereira, Direct conversion of cellulose to sorbitol over ruthenium catalysts: influence of the support, Catal. Today 279 (2017) 244–251.
[25] P.A. Lazaridis, S. Karakoulia, A. Delimitis, S.M. Coman, V.I. Parvulescu, K.S. Triantafyllidis, d-Glucose hydrogenation/hydrogenolysis reactions on noble metal (Ru, Pt)/activated carbon supported catalysts, Catal. Today 257 (2015) 281–290.
[26] L.S. Ribeiro, J.J. Delgado, J.J.M. Órfão, M.F.R. Pereira, Influence of the surface chemistry of multiwalled carbon nanotubes on the selective conversion of cellulose into sorbitol, ChemCatChem 9 (2017) 888–896.
[27] D. Wang, W. Niu, M. Tan, M. Wu, X. Zheng, Y. Li, N. Tsubaki, Pt nanocatalysts supported on reduced graphene oxide for selective conversion of cellulose or cellobiose to sorbitol, ChemSusChem 7 (2014) 1398–1406.
[28] M. Kumar, A.O. Oyedun, A. Kumar, A review on the current status of various hydrothermal technologies on biomass feedstock, Renewable Sustainable Energy Rev. 81 (2018) 1742–1770.
[29] A. Shrotri, A. Tanksale, J.N. Beltramini, H. Gurav, S.V. Chilukuri, Conversion of cellulose to polyols over promoted nickel catalysts, Catal. Sci. Technol. 2 (2012) 1852–1858.
[30] A. Fukuoka, P.L. Dhepe, Catalytic conversion of cellulose into sugar alcohols, Angew. Chem. Int. Ed. 45 (2006) 5161–5163.
[31] J.M.A.R. Almeida, L. Da Vià, P. Demma Carà, Y. Carvalho, P.N. Romano, J.A.O. Peña, L. Smith, E.F. Sousa-Aguiar, J.A. Lopez-Sanchez, Screening of mono- and bi-functional catalysts for the one-pot conversion of cellobiose into sorbitol, Catal. Today 279 (2017) 187–193.
[32] G. Liang, C. Wu, L. He, J. Ming, H. Cheng, L. Zhuo, F. Zhao, Selective conversion of concentrated microcrystalline cellulose to isosorbide over Ru/C catalyst, Green Chem. 13 (2011) 839–842.
[33] M. Thommes, K. Kaneko, A.V. Neimark, J.P. Olivier, F. Rodriguez-Reinoso, J. Rouquerol, K.S.W. Sing, Physisorption of gases, with special reference to the evaluation of surface area and pore size distribution (IUPAC Technical Report), Pure Appl. Chem. 87 (2015) 1051–1069.
[34] A. Lecloux, J.P. Pirard, The importance of standard isotherms in the analysis of adsorption isotherms for determining the porous texture of solids, J. Colloid Interface Sci. 70 (1979) 265–281.
[35] H. Marsh, F. Rodríguez-Reinoso, Activation processes (thermal or physical), in: H. Marsh, F. Rodríguez-Reinoso (Eds.), Activated Carbon, Elsevier Science Ltd, Oxford, 2006, pp. 243–321.
[36] J.L. Figueiredo, M.F.R. Pereira, M.M.A. Freitas, J.J.M. Órfão, Modification of the surface chemistry of activated carbons, Carbon 37 (1999) 1379–1389.
[37] J.L. Figueiredo, M.F.R. Pereira, M.M.A. Freitas, J.J.M. Órfão, Characterization of active sites on carbon catalysts, Ind. Eng. Chem. Res. 46 (2007) 4110–4115.
[38] R.P. Rocha, O.S.G. Soares, J.L. Figueiredo, M.F.R. Pereira, Tuning CNT properties for metal-free environmental catalytic applications, Journal of Carbon Research 2 (2016).
[39] J. Zhou, Z. Sui, J. Zhu, P. Li, D. Chen, Y. Dai, W. Yuan, Characterization of surface oxygen complexes on carbon nanofibers by TPD, XPS and FT-IR, Carbon 45 (2007) 785–796.
[40] H.F. Gorgulho, J.P. Mesquita, F. Gonçalves, M.F.R. Pereira, J.L. Figueiredo, Characterization of the surface chemistry of carbon materials by potentiometric titrations and temperature-programmed desorption, Carbon 46 (2008) 1544–1555.
[41] N. Rey-Raap, M. Enterría, J.I. Martins, M.F.R. Pereira, J.L. Figueiredo, Influence of multiwalled carbon nanotubes as additives in biomass-derived carbons for supercapacitor applications, ACS Appl. Mater. Interfaces 11 (2019) 6066–6077.
[42] Y. Chen, C. Liu, F. Li, H. Cheng, Pore structures of multi-walled carbon nanotubes activated by air, CO2 and KOH, J. Porous Mater. 13 (2006) 141–146.
[43] X. Guo, H. Dong, B. Li, L. Dong, X. Mu, X. Chen, Influence of the functional groups of multiwalled carbon nanotubes on performance of Ru catalysts in sorbitol hydrogenolysis to glycols, J. Mol. Catal. A Chem. 426 (2017) 79–87.
[44] Y. Weng, S. Qiu, C. Wang, L. Chen, Z. Yuan, M. Ding, Q. Zhang, L. Ma, T. Wang, Optimization of renewable C5 and C6 alkane production from acidic biomass hydrolysate over Ru/C catalyst, Fuel 170 (2016) 77–83.
[45] D. Rochefort, P. Dabo, D. Guay, P.M.A. Sherwood, XPS investigations of thermally prepared RuO2 electrodes in reductive conditions, Electrochim. Acta 48 (2003) 4245–4252.
[46] Z. Li, Y. Liu, C. Liu, S. Wu, W. Wei, Direct conversion of cellulose into sorbitol catalyzed by a bifunctional catalyst, Bioresour. Technol. 274 (2019) 190–197.
[47] S. Van de Vyver, J. Geboers, W. Schutyser, M. Dusselier, P. Eloy, E. Dornez, J.W. Seo, C.M. Courtin, E.M. Gaigneaux, P.A. Jacobs, B.F. Sels, Tuning the Acid/Metal balance of carbon nanofiber-supported nickel catalysts for hydrolytic hydrogenation of cellulose, ChemSusChem 5 (2012) 1549–1558.
[48] P.A. Lazaridis, S.A. Karakoulia, C. Teodorescu, N. Apostol, D. Macovei, A. Panteli, A. Delimitis, S.M. Coman, V.I. Parvulescu, K.S. Triantafyllidis, High hexitols selectivity in cellulose hydrolytic hydrogenation over platinum (Pt) vs. ruthenium (Ru) catalysts supported on micro/mesoporous carbon, Appl. Catal. B 214 (2017) 1–14.